Author's post-print version of "O'Reilly, C., & Nielsen, T. (2013). Assessing EEG sleep spindle propagation. Part 1: Theory and proposed methodology. J Neurosci Methods. doi: 10.1016/j.jneumeth.2013.08.013" (http://www.sciencedirect.com/science/article/pii/S0165027013002847)

Title

Assessing EEG sleep spindle propagation. Part 1: Theory and proposed methodology

Authors

Christian O'Reilly, Ph.D & Tore Nielsen, Ph.D.
[christian.oreilly, tore.nielsen]@umontreal.ca

Dream and Nightmare Laboratory
Center for Advanced Research in Sleep Medicine
Hôpital du Sacré-Coeur de Montréal
5400 boulevard Gouin Ouest
Montréal, Québec
H4J 1C5, Canada

Keywords

electroencephalography; sleep spindle; time delay; time-frequency analysis; signal propagation; S-transform

Abstract

Background: A convergence of studies has revealed sleep spindles to be associated with sleep-related cognitive processing and even with fundamental waking state capacities such as intelligence. However, some spindle characteristics, such as propagation direction and delay, may play a decisive role but are only infrequently investigated because of technical difficulties.

New Method: A new methodology for assessing sleep spindle propagation over the human scalp using noninvasive electroencephalography (EEG) is described. This approach is based on the alignment of time-frequency representations of spindle activity across recording channels.

Results: This first of a two-part series concentrates on framing theoretical considerations related to EEG spindle propagation and on detailing the methodology. A short example application is provided that illustrates the repeatability of results obtained with the new propagation measure in a sample of 32 night recordings. A more comprehensive experimental investigation is presented in part two of the series.

Comparison with Existing Method(s): Compared to existing methods, this approach is particularly well adapted for studying the propagation of sleep spindles because it estimates time delays rather than phase synchrony and it computes propagation properties for every individual spindle with windows adjusted to the specific spindle duration.

Conclusions: The proposed methodology is effective in tracking the propagation of spindles across the scalp and may thus help in elucidating the temporal aspects of sleep spindle dynamics, as well as other transient EEG and MEG events. A software implementation (the Spyndle Python package) is provided as open source software.

1. Introduction

1.1. Importance of sleep spindle study

A convergence of studies has revealed that electroencephalographic (EEG) sleep spindles—0.5 to 3.0-second phasic bursts with an oscillatory activity in the 11 to 16 Hz range— are of clinical significance in contexts as varied as schizophrenia (Ferrarelli et al., 2010), stroke recovery, mental retardation, abnormal maturation (De Gennaro and Ferrara, 2003) and sleep deprivation (Knoblauch et al., 2003). They also have been associated with sleep-related cognitive processes such as memory consolidation (Schabus et al., 2004; Schabus et al., 2006) and waking state capacities such as intelligence (Fogel and Smith, 2011). They have been hypothesized to promote sleep by modulating the afferent impact of both external (Dang-Vu et al., 2010; Schabus et al., 2012) and internal (Doran, 2003) stimuli. Finally, sleep spindles have been recognized as playing a role in cortical development (Jones et al., 2006).

Different sleep spindle characteristics are associated with different properties of these conditions, processes, and capacities. Studies have shown: that density, amplitude, and duration of fast (13-15Hz) but not slow (10-13Hz) sleep spindles correlate with sleep-dependent improvements in visuomotor performance (Tamaki et al., 2008); that fast sleep spindles in frontal regions are of particular importance for memory consolidation (van der Helm et al., 2011); that spindle density, number, and coherence are lower in schizophrenia patients than in controls (Wamsley et al., 2012); and that spindle number, density, and duration are significantly reduced with normal aging (Crowley et al., 2002). Such examples show that new research avenues may depend on a better characterization of the electrophysiological qualities of sleep spindles. Although amplitude, density, and frequency are often used, other potentially useful characteristics, such as spindle propagation properties, are overlooked because of a lack of tools

for efficiently assessing them from standard polysomnographic recordings. In this paper, we present a novel methodology that provides such tools.

1.2. Spindle time-frequency analysis

Sleep spindles, and sleep in general, are investigated using predominantly polysomnographic recordings that necessitate the analysis of nonstationary signals. As such, this field is a natural candidate for time-frequency analysis, which quantifies temporal variation of the spectral content of nonstationary signals. Accordingly, time-frequency analysis has been applied in an increasing number of sleep EEG studies in recent years including: development of automatic sleep stage identification systems (Fraiwan et al., 2011), evaluation of developmental changes in human sleep (Tarokh and Carskadon, 2010), characterization of macroscopic and microscopic sleep features (Kokkinos et al., 2009), and investigation of periodic limb movements in REM and NREM sleep (Allena et al., 2009), to name a few. This signal processing approach has also been used more particularly to study the characteristics of sleep spindles (Andrillon et al., 2011; Ktonas et al., 2009).

The literature on time-frequency analysis proposes various mathematical tools that are potentially applicable to spindle analysis, such as the short-time Fourier transform, the spectrogram, the Hilbert-Huang transform, the Wigner-Vile distributions, the continuous wavelet transform, and the S-transform. These have complementary strengths and weaknesses and differential suitability for different classes of problems (Assous and Boashash, 2012). The S-transform (Stockwell et al., 1996) has been used for studies analyzing EEG signals (e.g., Jones et al., 2006; Pinnegar et al., 2009; Senapati and Routray, 2011) and offers several advantages for spindle analysis, including a low computational complexity (Brown et al., 2010), a direct relationship to the well-known Fourier spectrum (e.g., as opposed to wavelets), a well-

understood theoretical foundation (e.g., as opposed to the Hilbert-Huang transform), an easy interpretation (e.g., no cross-term ambiguities such as in bilinear time-frequency distributions), and a time-resolution that is adjusted as a function of frequency (e.g., as opposed to the spectrogram).

1.3. EEG propagation analysis

In this paper we extend our development of a methodology to track the propagation of transient EEG waveforms over the scalp (O'Reilly and Nielsen, 2013b) and tailor it to the specific application of sleep spindle propagation.

This topic, and the remotely related topic of spindle source localization, have been addressed using invasive methods in epileptic subjects (Andrillon et al., 2011) and animals (Steriade, 2000). It has also been investigated using low-resolution brain electromagnetic tomography (LORETA) (Anderer et al., 2001; Ventouras et al., 2010) and similar techniques (Caporro et al., 2012; Schabus et al., 2007; Tyvaert et al., 2008). Furthermore, different techniques have been developed to investigate properties of the propagation of EEG activity: coherence, Granger causality (Granger, 1969), directed transfer function (DTF) (Kaminski and Blinowska, 1991), partial directed coherence (Sameshima and Baccala, 1999), synchronization likelihood (Stam and van Dijk, 2002), phase lag index (PLI) (Stam et al., 2007), imaginary part of coherency (Nolte et al., 2004), comparison of phase delay on slow waves (<1 Hz) (Massimini et al., 2004), etcetera. However, most of these latter techniques are oriented toward the study of functional connectivity between brain regions. These estimations generally rely on the average activity of large recording epochs (e.g., to study spontaneous activity during a resting state) or on the average of multiple windowed signal sections of constant size (e.g., to

study typical brain reactivity to a time-locked stimulus). These techniques were not designed to analyze the propagation of individual[1], spontaneously-occurring, transient events of variable duration such as sleep spindles. Moreover, many of these techniques mainly address phase synchronization. This can cause problems in estimating propagation delays since the phase shift between the activity of two signals is ambiguously linked to propagation delay, the phase repeating itself every $\frac{1}{f}$ second, with f representing the signal frequency in Hertz.

Thus, in this paper we propose a new methodology more adapted to the tracking of topographical displacements of EEG sleep spindles. This approach has the following properties: 1) it is noninvasive, 2) it relies on standard EEG recordings only (e.g., it does not need expensive and time consuming scanning procedures), 3) it is geared toward the estimation of time delays rather than phase synchrony, 4) it uses analysis windows of variable size depending on the duration of the spindles, and 5) it computes propagation properties for individual spindle, rather than for average spindle, behavior.

To meet these requirements, we propose a methodology that describes the propagation of spindle waves using the S-transform and a cross-correlation of time-frequency representations, similar to what has been proposed in the context of matched filters (Flandrin, 1988; O'Toole et al., 2005)[2]. By comparing the information captured from different EEG channels, we track spindles across the scalp and assess their propagation delays and directions.

[1] See however the work of Doran (2003) who studied the dynamic topography of individual sleep spindles rather than characteristics of average recording epochs, much as we propose here.

[2] Matched filters are obtained by correlating a signal template to an incoming signal to find occurrences of the template within the incoming signal. Originally developed for the temporal domain, it has also been applied to time-frequency representations. Although conceptually close to this technique, our approach is

In this approach, the cross-correlation is preferred to coherence because it avoids possible ambiguities associated with the conversion of phase shifts in time delays. Also, time-frequency rather than time representations are cross-correlated following the hypothesis that features of EEG transient waveforms may be more easily distinguished with the time-frequency representation. This hypothesis is motivated by the fact that sleep spindles are generally described with both frequency features (intra-spindle oscillation at frequencies between 11-16 Hz; a generally decreasing frequency from the onset to the offset) and temporal features (0.5 to 3.0 second duration, a waning and waxing pattern). Analyzing the spindle phenomenon only in frequency space is problematic because of nonstationarity. Similarly, analyzing only its temporal representation also can cause problems. Evaluating the similarity of signals using temporal cross-correlation can give spurious estimations because similar signals that differ only by slightly different fundamental frequencies will drift out of phase over time and will show only a low cross-correlation despite their similarity. Thus, spindles are ideally investigated in a representation space that allows monitoring of spectral activity as it varies over time.

1.4. Overview

In the following section, a theoretical framework for this methodology is presented. Its adoption seems essential for properly interpreting EEG propagation since the latter is qualitatively different from propagation through the axonal pathways of neural networks as measured by

---

mathematically different as it computes a normalized index of similarity and it performs the cross-correlation of time-frequency spectra only along the temporal axis, as discussed further in section 3.

indwelling electrodes, e.g., Andrillon et al. (2011). Section 3 presents in detail the different steps necessary to compute and analyze sleep spindle propagation over the scalp with this methodology. Section 4 provides results obtained with this methodology while section 5 concludes the paper. Readers interested by a more in-depth experimental assessment and validation of this EEG spindle propagation methodology can consult an extension of the present work (O'Reilly and Nielsen, 2013a).

2. Theoretical framework: Spindles as transient brain waves

Just as light has been usefully, albeit paradoxically, described as both particles in flux and electromagnetic waves, so too may complementary views of brain activity be useful in understanding and studying such activity. The distinction between neural networks, or cell assemblies, and global fields of synaptic action (Nunez and Srinivasan, 2006) is one such framework that helps situate the use of EEG analysis in our approach. These authors distinguish cell assemblies which they rather loosely define as "any group of neurons or neural masses (*minicolumns, corticocortical columns, macrocolumns*, and so forth) for which preferential interactions persist over time intervals of perhaps several tens of milliseconds or more" (p. 24) and *synaptic potential fields* which they consider as spatially and temporally localized cumulative consequences of the activity of a large number of neurons, regardless of their connectivity. These two different views are necessary to apprehend the human brain from different levels of abstraction and different recording scales, at least for three reasons.

First, because of the distance between neural activity and electrodes, the size of electrodes, and the effect of volume conduction smearing by cerebrospinal fluid, skull, and other tissues, EEG signals record large-scale information about the global fields of synaptic

action rather than smaller scale activity associated with specific cortical or thalamocortical networks (Nunez and Srinivasan, 2006). Although, there is no agreement on how large of a scale EEG recording are, investigators agree on the fact that very large pools of synchronously active neuronal cells (60,000,000 for Nunez and Srinivasan (2006), 10,000-50,000 for Murakami and Okada (2006)) covering a substantial cortical area (6 cm^2 for Nunez and Srinivasan (2006), 0.25 cm^2 for Baillet et al. (2001)) are necessary to generate electrical fields that are recordable over the scalp. Further, although source localization can be performed successfully using an appropriate recording array density, inverse EEG modeling, and realistic MRI-based reconstruction (see Michel et al. (2004) for a review), equivalent current dipoles must be considered as a mathematically simplified account of neuronal activity spreading over an area somewhere between ¼ and 6 square centimeters of cortex and not as a focal neural activation (Nunez and Srinivasan, 2006; Salmelin and Baillet, 2009). Thus, as standard polysomnographic recording provides a rather large-scale estimate of synaptic action, attempts to analyze EEG sleep spindle activity in direct relation to neuronal networks might lead to confusion. Such finer-scale investigations are better approached with electrocorticography or implanted electrodes.

Second, there is some evidence (e.g., Plonsey, 1982) that the EEG might only be recording electrical fields associated with secondary volume current (return currents resulting from the reaction of the extracellular environment to the primary current), and not with the primary neurophysiologically driven currents that are generally of interest. This important point is seldom discussed in the literature although some modeling efforts, e.g., the ELECTRA source model of Grave de Peralta Menendez et al. (2000), try to take it into account .

Third, Nunez and Srinivasan (2006) discuss how the activity of global synaptic and action potential fields recorded in the EEG display wave-like activity that may facilitate neural network interactions by helping the coordination of separate functions in unified behavior and

consciousness. Such a mechanism is of particular interest for the study of sleep spindles given their known association with learning and IQ.

Thus, on the one hand, there are good reasons to investigate EEG activity as a measure of global synaptic and action potential fields. On the other hand, scalp EEG recordings show sleep spindle oscillations traveling over the scalp for relatively small distances with relatively short time delays (O'Reilly and Nielsen, 2013a). Therefore, it seems appropriate to model the transient EEG activity of sleep spindles as a wave-like dynamic emerging from global synaptic potential fields. The remainder of this paper concentrates on rigorously defining a methodology to asses spindle propagation in this particular theoretical context.

3. Methodology : Assessment of spindle propagation

3.1. Spindle detection

A standard channel-per-channel spindle detection is prerequisite to spindle propagation analysis. Detection can be performed by experts or by automated algorithms, but experts are typically taken to represent the gold standard. Nonetheless, the inter-scorer reliability of experts is considered low at around 86% (Campbell et al., 1980). Expert scoring may be affected by subjective factors such as expectation, fatigue, motivation, general mood, and level of expertise, and experts may miss hidden spindles that automated detectors would detect. Also, consistency in spindle scoring is complicated by overnight changes in the signal-to-noise ratio of background sigma activity as well as by the large variability of sleep spindle characteristics (frequency, duration, amplitude) attributable to the individual, the sleep stage, the sleep cycle, and the topographical localization of recording electrodes. To minimize false detections by human scorers, one suggested approach is to consider only spindles that have been detected

independently by more than one expert (Campbell et al., 1980; Morrow and Casey, 1986; Ray et al., 2010). A drawback of this approach is that it necessitates duplicating the detection process by more than one scorer – a tedious and time-consuming task. Other suggested methods of improving reliability include aiding visual detection with duplicate channels that display typically filtered EEG alongside EEG that is bandpass filtered in the spindle frequency range (Ray et al., 2010). To what extent such technical and methodological advances will succeed in improving significantly the inter-rater agreement in years to come is difficult to assess at present. Most probably, manual scoring will progress toward semi-automation benefitting from further advances in signal processing.

On the other hand, automated detectors often produce large proportions of false detections relative to expert scorers. As discussed previously (O'Reilly and Nielsen, 2013c), this can be a significant problem for assessing spindle characteristics because, in such cases, average statistics are computed on samples that contain a large proportion of non-spindle signals. However, in many cases, this problem can be reduced by adjusting detector parameters (e.g., decision threshold values). Such parameters generally allow choosing an operating point in the tradeoff between precision (also known as the positive predictive value) and sensitivity (also known as the true positive rate). When using such detectors to assess spindle characteristics, it might be preferable to put more emphasis on precision rather than sensitivity so as to minimize the false detection rate. Indeed, failing to detect some real spindles may reduce statistical power by shrinking the spindle pool (increased type II error) but including excessive false detections may create biased or artifactual findings (increased type I error), a more serious situation. However, caution is nevertheless advised since favoring precision might also create a population selection bias if a stricter threshold rejects positive cases unevenly across different subpopulations of spindles.

It is noteworthy that this tradeoff selection dilemma is a fundamental property of the diagnostic problem. Although adaptive algorithms or parameters (e.g., a 95th percentile root mean square amplitude cut-off instead of a fixed value such as 25 μV) can be used to decrease both types of error simultaneously, there are always tradeoff parameters to adjust (e.g., the choice of using the .95 versus the 0.93 percentile).

In the absence of a definitive and highly reliable gold standard for spindle scoring, the final choice of scoring method is left to the experimenter. However, the adoption of a spindle scoring approach with a fine temporal resolution (see (O'Reilly and Nielsen, 2013c) for further discussion) is suggested so that the onsets and offsets of spindles are well localized in time.

3.2. Outline

The Python programming language was chosen to develop the spindle propagation software. The developed code is freely available for personal, educational, and research purposes as open source software. This software can be used directly with Stellate Harmonie (Stellate systems, INC., San Carlos, California, USA) .sig files or with standard European Data Format (EDF+/BDF+) files. For other formats, files must be converted to the EDF+/BDF+ format or code that allows the importation of raw EEG signals and annotations related to spindle scoring must be written. More information can be found at https://bitbucket.org/christian_oreilly/spyndle.

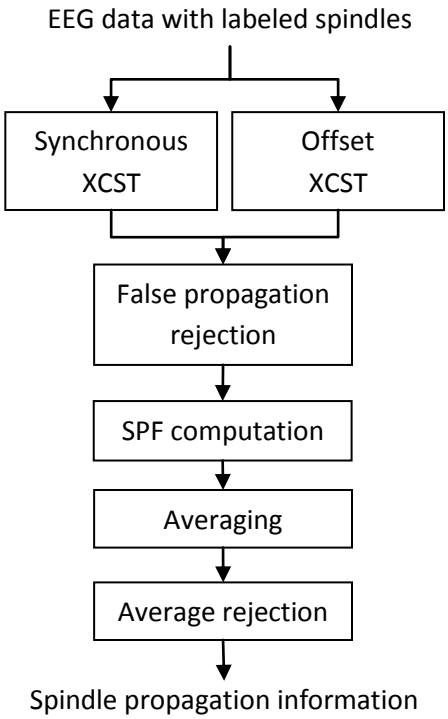

Figure 1. Outline of the spindle propagation assessment methodology.

Figure 1 shows a block diagram of the developed methodology. After spindles have been scored, the EEG stream is sent to a module computing the 2D cross-correlation of S-transform spectra (XCST) between a reference channel (the channel on which the spindle was detected) and a test channel (any other channel). The S-transform and the XCST algorithm are described in sections 3.3 and 3.4 respectively. The cross-correlation operation is performed with both synchronous and asynchronous (or offset) reference and test signals. As explained in section 3.5, the subsequent step (false propagation rejection) draws on information from synchronous and asynchronous comparisons to determine whether or not it is statistically probable that the synchronous comparison between reference and test channels reflect spindle propagation. Comparisons that are unlikely to reflect propagation are rejected before proceeding to the next step (*SPF computation*) where information concerning a single spindle, but gathered from different reference channels, is merged. As discussed more thoroughly in section 3.6., the entity

constructed by this merging operation is referred to as the *spindle propagation field* (SPF). Once SPFs have been computed, the propagation delays are averaged for every pair of electrodes and for every recording night. Averaged delays that are not statistically robust are subsequently rejected (section 3.7) and the spindle propagation information is output.

3.3. S-transform representation of sleep spindles

The well-known and widely used Fourier transform allows computation of the spectrum of a stationary signal that is sampled over a complete cycle for periodic signals or, theoretically, infinitely for non-periodic signals. Such a technique is poorly adapted to the study of nonstationary EEG signals, whose spectral content varies over time. The S-transform, and time-frequency analysis in general, allows the study of such signals by depicting variation of the spectrum as a function of time.

Figure 2 shows a typical result for time-frequency analysis of a single sleep spindle using the S-transform. The 2-dimensional color-coded representation shows variation of the spectrum amplitude as a function of both time and frequency.

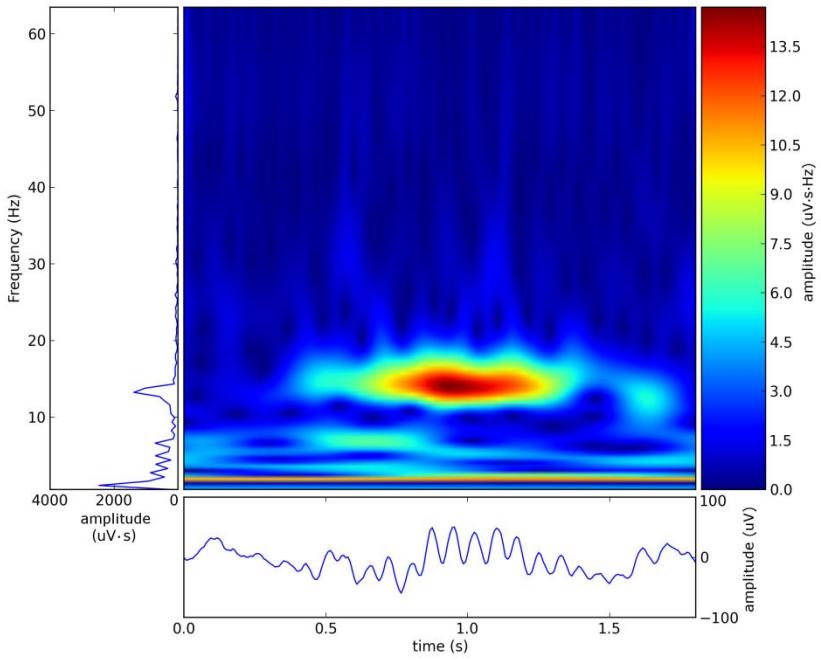

Figure 2. S-transform of a typical spindle-bearing EEG signal. Spindle activity in the 11-16 Hz band is visible between 0.5 and 1.5 seconds.

Conceptually, the S-transform corresponds to a short-time Fourier transform (i.e., a Fourier transform computed over short time periods of arbitrary duration but typically containing a few tens of milliseconds using a sliding window) with a Gaussian window function whose width varies inversely with signal frequency. Formally, this transform is expressed as

$$S(t,f) \stackrel{\text{def}}{=} \int_{-\infty}^{+\infty} h(\tau) \frac{|f|}{\sqrt{2\pi}} e^{-\frac{(t-\tau)^2 f^2}{2}} e^{-i2\pi f \tau} d\tau \qquad (1)$$

with t and f being transform time and frequency and $h(\tau)$ being the signal to be transformed (Stockwell et al., 1996).

3.4. Spindle propagation analysis

To evaluate the time delay of a spindle propagating from a reference channel C_R to a test channel C_T, we first compute the S-transform of the C_R and C_T EEG signals over the $f_\sigma = [f_{\sigma-}, f_{\sigma+}]$ frequency band – taken here as being equal to 11-16 Hz – and the time interval I defined as

$$I \stackrel{\text{def}}{=} [t_{sb} - \Delta_{sp} - \Delta_w, t_{se} + \Delta_{sp} + \Delta_w] \quad (2)$$

where t_{sb} and t_{se} are respectively the spindle beginning and ending times, Δ_{sp} is a padding time interval used to define an analysis window covering slightly more than the spindle duration, and Δ_w is another time interval used to allow sufficient room for sliding the window of analysis to compare C_R and C_T signals (see later). In our computations, we used $\Delta_{sp} = \Delta_w = 0.5$ seconds. The padding Δ_{sp} is used according to the hypothesis that the time-frequency pattern shortly before and after the sleep spindle is generally more closely related to the spindle (irrespective of the channel on which this spindle is recorded) than to activity that is not associated with this spindle. This is partly supported by the observation that MEG spindle activity spans a longer time interval than what can be seen with the EEG (i.e., starting ~150 ms before the EEG spindle activity and ending ~250 ms after it, according to Dehghani et al. (2011a)). This suggests that there is an associated process acting on a wider time window that could result in correlated activity in different channels within regions just preceding or following the detected EEG spindle activity. Thus, it is thought that adding this padding area may help in locating the propagation of the spindle across channels.

For simplicity, we label $|S_R(t,f)|$ and $|S_T(t,f)|$, respectively, the modulus[3] of the two previously computed S-transforms. We also note $\widetilde{S_x}(\Delta_t)$ a S-transform $S_x(f,t)$ time-shifted by a delay Δ_t such that $\widetilde{S_x}(\Delta_t) \equiv S_x(t+\Delta_t, f)$. An index of similarity between the activity on channels C_R and C_T with an offset Δ_t can be computed using

$$X_f(\Delta_t) = \frac{|\,\widetilde{S_R}(0)| \star |\widetilde{S_T}(\Delta_t)|}{L_p(|\widetilde{S_R}(0)|, |\,\widetilde{S_T}(\Delta_t)|)} \tag{3}$$

where the $\star$ symbol represents the following integral

$$\widetilde{F_1}(t_1) \star \widetilde{F_2}(t_2) \stackrel{\text{def}}{=} \int_{f_{\sigma-}}^{f_{\sigma+}} \int_{t_{sb}-\Delta_{sp}}^{t_{se}+\Delta_{sp}} F_1(t+t_1, f) F_2(t+t_2, f)\, dt df. \tag{4}$$

and $L_p(x,y)$ is the p-norm of the vector $[x \star x, y \star y]$.

One should note that, by using (4) for performing a one-dimensional cross-correlation of 2D signals, we decided to consider the *intra-spindle mean frequency*[4] as an intrinsic spindle property; its value is considered to be unaffected by propagation. Investigators wishing to postulate different a priori hypotheses about spindle propagation could generalize the approach by performing cross-correlations in two dimensions (i.e., both in time and frequency) to simultaneously study the time delay and the frequency shift associated with spindle spatial propagation.

Although some results suggest strong correlations between spindle occurrences of different intra-spindle mean frequencies (Dehghani et al., 2011b; Molle et al., 2011), we

[3] The modulus here is taken as the Euclidean norm of the S-transform complex representation. That is, for $S_R(t,f) = x + yj$, we consider the modulus given by $|S_R(t,f)| = \sqrt{x^2+y^2}$.

[4] The intra-spindle mean frequency can be defined in different ways, but a conceptually and computationally simple definition is to consider the frequency with the highest amplitude in the spectrum of spindle Fast Fourier Transform.

consider here that two time-locked spindles with important time delays (e.g. 500 ms) and with different mean frequencies should not be considered as being the propagation of a single spindle but as being two different spindles whose generations are time-locked. Although this probably indicates functional connectivity between these two regions, we do not consider it as indicating a phenomenon of EEG spindle propagation from one region to another.

Concerning the p-norm $L_p(x, y)$ used in (3), the infinity norm

$$L_\infty(x, y) \stackrel{\text{def}}{=} max(x \star x;\ y \star y) \tag{5}$$

and the Euclidean norm

$$L_2(x, y) \stackrel{\text{def}}{=} \sqrt{(x \star x)^2 + (y \star y)^2} \tag{6}$$

are two cases of special interest. Whereas (5) penalizes the comparison of spindles of the same shape but different amplitudes, (6) does not. Ultimately, the choice of one norm over the other rests on an a priori hypotheses regarding whether the amplitude of a given spindle changes during propagation. Although mean spindle amplitude depends on its scalp location, this does not mean that the amplitude of individual spindles varies when it propagates; its variation could be due solely to a different mean amplitude of the spindle detected at a particular location, regardless of the behavior of amplitude during propagation. For the present work, we chose to use amplitude as an intrinsic property of a given spindle (i.e., not varying during propagation) and hence, chose the norm L_∞.

With definition (4), applying L_∞, $X_f(\Delta_t)$ represents the cross-correlation between $S_R(0)$ and $S_T(\Delta_t)$ normalized by whichever value is greater in the autocorrelations of $|S_R(0)|$ and $|S_T(\Delta_t)|$. In this context, $X_f(\Delta_t)$ can be considered as an index of resemblance between $|S_R(0)|$ and $|S_T(\Delta_t)|$, normalized to the [0, 1] range. This would also have been the case if we

had chosen L_2 since the Cauchy–Schwarz inequality ensures that L_2 also results in a normalized [0, 1] range (see the Appendix for a demonstration).

Using this normalized cross-correlation, the S-transformed signal of the reference channel centered around the spindle occurrence (i.e., $|S_R(0)|$) is compared to a sliding window of the S-transformed signal of a test channel. This window is moved along the time axis by varying the value of Δ_t from $-\Delta_w$ to $+\Delta_w$ in steps of $1/f_s$, f_s being the sampling frequency. Figure 3 illustrates this comparison process.

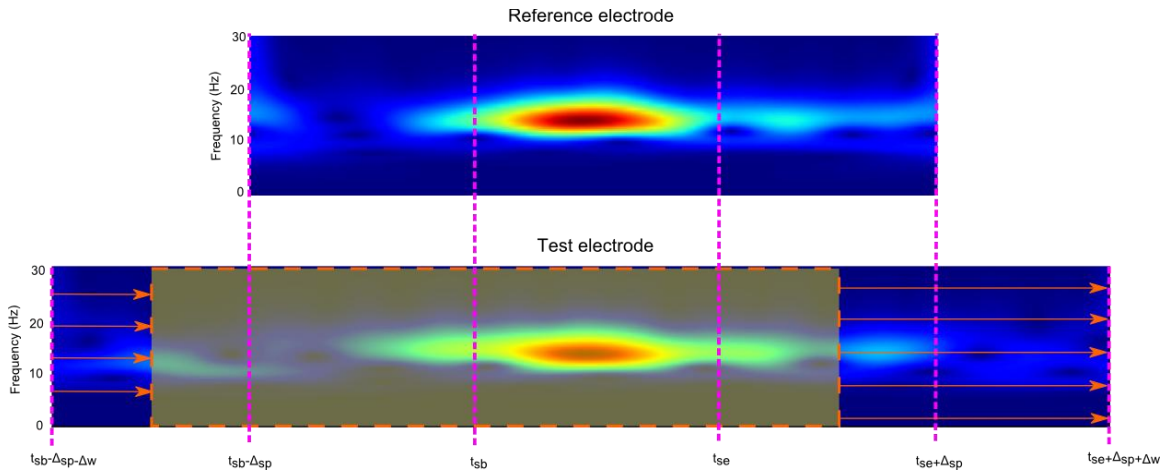

Figure 3. Illustration of the process of computing the similarity between$|\boldsymbol{S_R(0)}|$ (upper panel) and $|\boldsymbol{S_T(\Delta_t)}|$ (lower panel). The translucent yellow box shows the window of comparison sliding along the time axis according to the value of $\boldsymbol{\Delta_t}$.

Once the $X_f(\Delta_t)$ curve has been computed, we seek the value Δ_t^* that maximizes this function. This value corresponds to the delay between C_R and C_T for which the signals of reference and test channels have the most similar time-frequency content. Accordingly, $X_f(\Delta_t^*)$ represents the degree of similarity for this adjustment, with 1.0 being obtained for two identical signals and 0.0 being obtained for two completely dissimilar signals (i.e., two signals h_1 and h_2 such that $h_1 = 0$ whenever $h_2 \neq 0$ and vice-versa).

Using this methodology, each spindle automatically detected on each channel can be compared to the signal recorded on all other channels. At the conclusion of this process, the algorithm provides the delays Δ_t^* (taken in a possible range from $-\Delta_w$ to $+\Delta_w$ seconds) for the optimal fitting between the S-transforms of each spindle detected on each reference channel and the S-transforms of the signal recorded on every other channel. However, if a spindle does not propagate from the reference electrode to the test electrode, then the estimated delay is meaningless. These cases can be referred to as false positives (FP) as they have detected a correspondence between C_R and C_T when such a relationship does not exist. FPs should result in a low value of $X_f(\Delta_t^*)$ (i.e., a spindle picked up by the reference electrode does not correspond to the same spindle picked up by the test electrode) indicating a poor similarity between signals of the reference and the test channels.

3.5. Spindle similarity and false positive rejection

At this stage, we define how similar two signals must be for us to conclude that they reflect activity of one and the same spindle. In practice, we require a threshold λ such that we are confident there is spindle propagation between two electrodes if $X_f(\Delta_t^*) > \lambda$. To define such a threshold, we use the previously described methodology to compare C_R and C_T but apply a time offset of five seconds on C_T such that all comparisons will be between a spindle on C_R and an unrelated signal on C_T. Although this offset C_T signal might contain other spindles, because of the five-second delay it cannot contain the spindle under investigation on C_R. These comparisons between the C_R signal and the offset C_T signal will henceforth be referred to as offset comparisons, as opposed to the synchronous comparisons obtained previously between C_R and the non-offset C_T signals. It should be noted that although we systematically apply a positive offset on C_T, no bias results from this manipulation. To test this, we applied a negative

five-second delay and observed results that were qualitatively the same as with a positive five-second delay.

Once these offset comparisons are computed, their density function provides an estimate of the FP density function. Thus, a threshold can be fixed such that it rejects FP with a confidence of $(100 - \alpha)\%$ ($\alpha = 10$ in our analyses). Figure 4 illustrates this process.

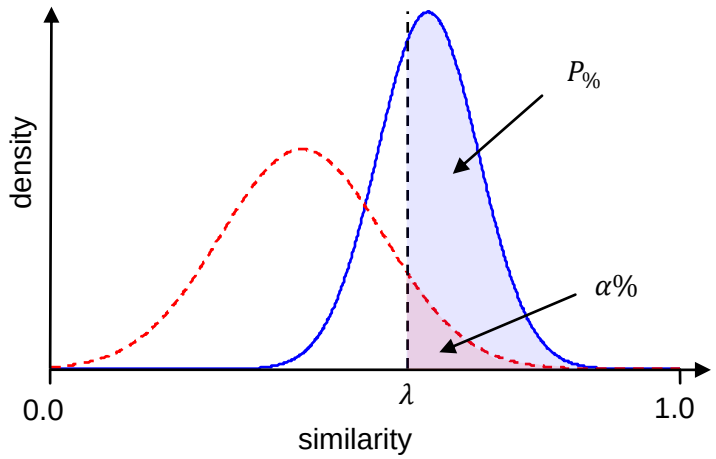

Figure 4. Definition of the $\boldsymbol{\lambda}$ threshold. The red and blue curves are associated with the offset and synchronous comparisons respectively. Because of the offset, the red curve estimates the density of FP whereas the blue curve is based on synchronous comparisons and thus contains a mixture of true and false positives. The threshold $\boldsymbol{\lambda}$ is set such that only α% of the area under the red curve falls to the right tail. Note that Gaussian density functions have been used in this figure for simplicity, but this technique is nonparametric. The distribution of $\boldsymbol{X_f(\Delta_t^*)}$ does not need to be, and in most cases is not, Gaussian. See text for further details.

In this figure, the density distribution of the value of $X_f(\Delta_t^*)$ for the offset comparison is shown in red while the density for the non-offset comparison is shown in blue. We set a threshold at the value λ (shown as a vertical dashed line) such that only α% of the area under the red curve is at the right of this threshold (the portion shown in pink). The portion of the blue

curve for which $X_f(\Delta_t^*) > \lambda$ is shown in light blue. The percentage of area under the curve covered by this portion is labeled $P_{\%}$ and contains all comparisons that are considered valid. These comparisons can be referred to as positive (P), i.e., are composed of the true positive (TP) and the FP that we failed to reject.

In section 4.3., the λ threshold is shown to vary as a function of the subject, reference channel, and test channel. Thus, a first rejection criterion (C_1) should be applied using

$$C_1: X_f(\Delta_t^*) \leq \lambda \tag{7}$$

with a different value of λ computed for every combination of subject, reference channel, and test channel.

The expected proportion of FP not rejected by this criterion (i.e., or equivalently, the false detection rate) is equal to

$$FDR = \frac{\alpha\kappa}{P_{\%}} = \kappa\widetilde{FDR} \tag{8}$$

with κ being the proportion of FP in the sample before the application of the criterion and $P_{\%}$ the proportion of the area of the blue curve that falls to the right of λ as shown in Figure 4. In the case where the sample contains only FP ($\kappa = 1$), we expect $P_{\%}$to equal α on average, such that $FDR = 1.0$. An upper bound on FDR can be estimated as $\widetilde{FDR} = {}^{\alpha}/_{P_{\%}}$. This upper bound has a minimal value of α, obtained when $P_{\%} = 1.0$. As it is not clear how the value of κ can be estimated, we can only rely on $\widetilde{FDR}$. This value should be kept small enough to have only a negligible effect on the average value of Δ_t^*. An empirical evaluation of the value of $\widetilde{FDR}$ is presented in section 4.4.

3.6. Statistical outlier rejection

A second criterion (C_2) is also applied to remove data points with statistically aberrant values of Δ_t^* according to a nonparametric test proposed by Tukey (1977). This test states that a particular value x_i of a random variable X is an outlier if

$$C_2: x_i > Q_3 + 1.5(Q_3 - Q_1) \quad \text{or} \quad x_i < Q_1 - 1.5(Q_3 - Q_1) \tag{9}$$

where Q_3 and Q_1 are the third and the first quartiles of the distribution of X.

3.7. Correction for negative propagation delays

Negative propagation delays occur when spindles detected on a reference channel are, in fact, propagating from the test electrode toward the reference electrode instead of the reverse. As the methodology proposed up to this point does not take into account the fact that propagation delays must have strictly positive values, averaging computed delays at this step would only give a propagation tendency, i.e., a positive delay between O1 and Fp1 would only indicate that more spindles travel from O1 to Fp1 than the inverse or that, on average, propagation from O1 to Fp1 is longer than the inverse. Therefore, the computed averaged delays would not reflect expected spindle propagation time delays. To correct this situation, we invert the channel roles (i.e., test versus reference) that are initially attributed in function of the spindle scoring (i.e., the channel on which the spindle was scored was considered as the reference). For example, for our interpretation to be correct from a physical point of view, a propagation assessed as being from Fz (reference) to F4 (test) with a negative time delay $-\tau$ must be changed to a propagation from F4 (reference) to Fz (test) with a positive time delay τ.

3.8. Spindle tracking

The results gathered for each reference channel separately can be combined to obtain a more complete portrait of the propagation of spindle activity. To avoid confusion, we will term this global picture the *spindle propagation field* (SPF) . To summarize: there are sleep spindles detected independently on separate electrodes that can be related or not to a singular underlying physiological event. For all these detected spindles, there can be one or many propagations. The set of spindles detected on different electrodes and their propagations that can *reasonably* be hypothesized as being associated with a single physiological event forms the entity that we call the SPF.

For spindle propagations that have not been rejected according to rejection rules C_1 and C_2, a set of four criteria is defined to determine when it is *reasonable* to merge observations from different channels into a single SPF. The first two rules state that: two detected spindles and their computed propagations can be merged only if:

1) they share a *common channel*;
2) onset times on their respective reference channels differ by less than 500 milliseconds.

The first rule ensures that the activity of associated spindles occurs in neighboring regions of the scalp. The expression *common channel* refers to a channel that is – for both detected spindles – either the reference channel or a channel associated with the reference channel through propagation. Figure 5.a illustrates the application of this rule. It displays four hypothetical spindles detected on four different reference channels. The electrodes belonging to these reference channels (Fp2, Fz, P3, and Pz) are identified as colored filled circles whereas their computed propagations are illustrated by arrows, with heads indicating the direction of propagation (i.e., the direction of increasing propagation delays). In this figure, spindles

detected on P3 and Pz share five common channels (C3, Cz, P3, Pz, and O1) and thus respect rule #1. This is also true for Fp2 and Fz which share common channels Fp2, Fz, and F4. It is not, however, true for the spindle detected on Fp2 and the spindle detected on P3, which share no common electrodes.

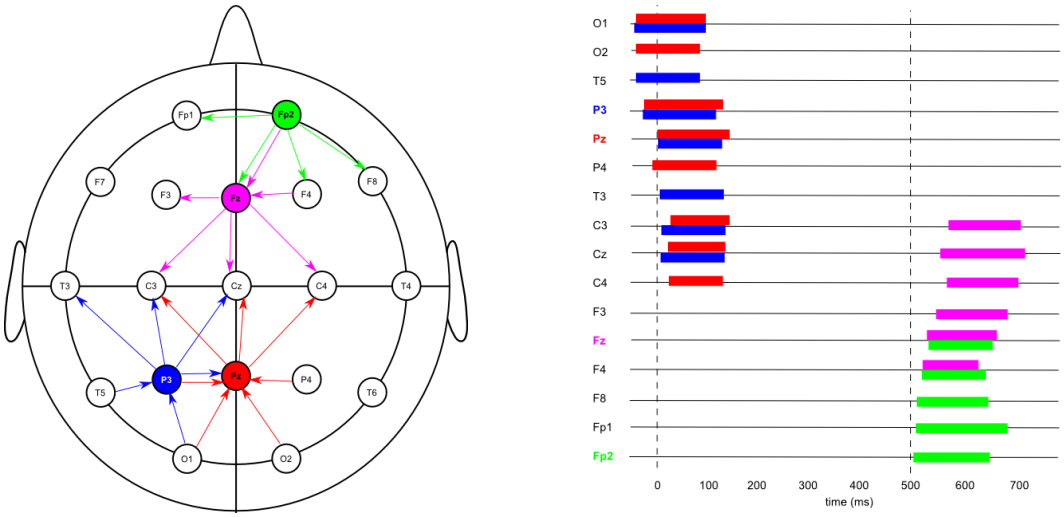

(a) (b)

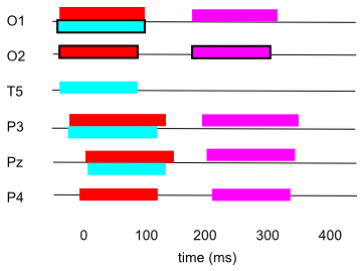

(c)

Figure 5. (a) Propagation trajectories for four hypothetical spindles. Electrodes belonging to the reference channels are colored. Arrows link reference and test channels, with the arrow head indicating the direction of spindle propagation. (b) Duration of spindles on all electrodes for the propagation schema depicted in (a). The detected spindles indicated by blue and by red respect rule #2, as do the spindles indicated by purple and by green. (c) Application of association rules

#3 and #4 for defining a spindle propagation field (SPF). Three detected spindles are identified using different colors, with black borders identifying the reference channel for each detected spindle. Because of temporal proximity the blue and red spindles form a single SPF but not the blue and purple spindles (rule #4). Because they both have the same reference channel, the red and purple spindles do not form a single SPF (rule #3).

The second rule ensures that associated spindles have a *close temporal occurrence*. Figure 5.b, illustrates the application of this rule. In this figure, the reference electrodes are indicated by bold and coloration of the channel labels at the right. Spindle duration is indicated with colored boxes spanning the onset and offset of spindle activity on each electrode. Rule #2 is met between the spindles detected on P3 (blue) and Pz (red) since the onset of spindle activity on Pz is separated by less than 500 ms from the onset of spindle activity on P3. The same holds for spindles detected on Fp2 and Fz, but not for spindles detected on Pz and P3.

Two supplementary association rules are necessary to avoid aberrant associations:

3) The activity of two detected spindles cannot be merged into a single SPF if they have the same reference channel.
4) When two detected spindles A and B have the same reference channel and they both could be merged with a detected spindle C, the association into a common SPF is made between C and the spindle whose onset is closer to the onset of C.

In Figure 5.c, three spindles are depicted with reference electrodes shown by black borders around the boxes reflecting the spindle durations. In this figure, rule #3 dictates that the red and the purple spindles cannot be associated because they have the same reference channel. In the same figure, rule #4 stipulates that the blue spindle will constitute a single SPF with the red

spindle but not with the purple spindle because the activity of the red and the blue spindles begin more closely in time.

Finally, for channel pairs of SPF characterized by two propagation delays, the average delay is considered. In Figure 5.a, this is the case between P3 and Pz and also between Fp2 and Fz.

3.9. Maximal reliable delay

Once FP comparisons and statistical outliers are removed and different observations of the same spindles are associated into single SPFs containing only positive propagation delays, we compute—for every recorded night—an average ($\overline{\Delta_t^*}$) and standard deviation ($sd(\Delta_t^*)$) of the time delays between each channel pairs. This is achieved with the fast Minimum Covariance Determinant (MCD) Estimator algorithm because it provides robust estimation with a high breakdown point (Rousseeuw and Van Driessen, 1999).

As we have set $\Delta_w = 0.5$ seconds, we know that after the reversal of propagation with negative time delays the value of Δ_t^* will be between 0 and 500 milliseconds. If no spindle propagation occurs between two electrodes and we are left with only FP propagation we would expect these delays to be distributed uniformly between 0.0 and 0.5 seconds. Such a distribution would have a standard deviation of 0.144 seconds. To proceed conservatively, we apply the following condition: we accept statistics on electrode-pairs if their standard deviations are one-fifth of this value. This corresponds to a standard deviation of 28.8 ms which would be obtained on a uniform distribution dispersed over 100 ms (instead of 500 ms) and which gives a 95% confidence interval of 114 ms when using a normal (instead of uniform) distribution assumption for the time delays. Thus, a further step of data filtering is to discard $\overline{\Delta_t^*}$ estimates according to the criterion C_3:

$$C_3: sd(\Delta_t^*) > 28.8\, ms \quad (10)$$

Moreover, we discard estimates of $\overline{\Delta_t^*}$ that are obtained with only a small number of valid (i.e., not rejected so far) spindles (hereafter, referred to as $N_{\Delta_t^*}$) because these small samples do not provide sufficient confidence in the estimation of $sd(\Delta_t^*)$. In the present exploratory study, we used

$$C_4: N_{\Delta_t^*} < 40 \tag{11}$$

as a fourth rejection criterion.

4. Results

4.1. Data collection

To illustrate use of this methodology, we applied it to 32 whole-night polysomnographic recordings from 13 women (26 ± 5.7 SD years old) and 4 men (23 ± 4.4 SD years old). Each subject slept for two consecutive nights in a hospital-based academic sleep laboratory; for two subjects, recordings from the second night are missing because of technical problems. Subjects were fitted with a 19-electrode montage (Fp1, Fp2,F3, F4, F7, F8, C3, C4, P3, P4, O1, O2, T3, T4, T5, T6, Fz, Cz, Pz) configured according to the international 10–20 system, and referenced to ear electrodes linked with a 10-kΩ resistance. EEG channels were sampled at 128 Hz using a Grass 12 Neurodata Acquisition System and nights were scored by expert polysomnographers according to AASM guidelines (Iber et al., 2007). Spindles were detected automatically using an in-house systems inspired by (Schimicek et al., 1994). A more detailed description of this subject sample and the experimental setup can be found in (O'Reilly and Nielsen, 2013a).

4.2. Assessable time delays

Our analyses revealed that $\overline{\Delta_t^*}$ and $sd(\Delta_t^*)$ are highly correlated ($\rho = 0.93$). In our dataset, the relationship between these statistics is accurately modeled by the equation

$$sd(\Delta_t^*) = 1.15\overline{\Delta_t^*} \quad (12)$$

Given this relationship, our choice of values for Δ_w limits the mean propagation delays that we can assess to mean time delays of approximately 25 ms.

4.3. Variability of the λ threshold

The λ threshold may vary depending on factors such as subject, night, reference channel, and test channel. In fact, the percentages of variance of λ that are associated with each of these factors were evaluated and the computed values are reported in The expected pr. As can be seen, the recording night has relatively little effect whereas the interaction between reference and test channels accounts for most of the λ variability. As discussed in section 3.5, this warrants the computation of individual λ for each experimental condition (subject, reference channel, test channel).

Table 1. Percent of variance of $\boldsymbol{\lambda}$ explained by different experimental factors.

Factor	Night	Subject	Reference channel	Test channel	Interaction
variance of λ explained	0.017%	1.94%	23.9%	34.9%	75.2%

4.4. Estimated upper bound on the expected false detection rate

For every pair of channels, the MCD method was used to compute robust estimation of the mean and standard deviation (SD) – across the 32 recording nights – of the upper bound on the expected false detection rate ($\widetilde{FDR}$). Obtained averages are listed in Table 2.

Table 2. Average $\widehat{FDR}$ computed using the robust MCD estimator. Row labels indicate the reference channel and column labels the test channel. Pairs of adjacent electrodes are shown in bold and underlined. Pairs of non-adjacent electrodes with an average $\widehat{FDR}$ between 0.1 and 0.2 are highlighted in grey.

	C3	C4	Cz	F3	F4	F7	F8	Fp1	Fp2	Fz	O1	O2	P3	P4	Pz	T3	T4	T5	T6
C3		0.14	**0.11**	**0.13**	0.23	**0.46**	0.59	0.32	0.47	**0.15**	0.26	0.52	**0.11**	0.15	**0.13**	**2.31**	1.60	**1.05**	1.20
C4	0.15		**0.11**	0.27	**0.13**	0.59	**0.42**	0.46	0.41	**0.14**	0.37	0.53	0.16	**0.12**	**0.13**	1.37	**3.05**	0.93	**1.57**
Cz	**0.19**	**0.16**		**0.20**	**0.21**	0.90	0.75	0.66	0.68	**0.15**	0.88	1.15	**0.24**	**0.17**	**0.12**	2.67	2.82	2.10	2.32
F3	**0.15**	0.26	**0.17**		0.18	**1.80**	0.67	**0.63**	0.43	**0.11**	0.55	0.68	0.30	0.38	0.31	**3.00**	1.67	1.12	1.24
F4	0.27	**0.15**	**0.17**	0.19		0.78	**0.93**	0.54	**0.74**	**0.11**	0.65	0.79	0.37	0.33	0.32	1.62	**3.38**	1.10	1.41
F7	**0.16**	0.28	0.21	**0.11**	0.28		0.32	**0.11**	0.25	0.19	0.39	0.50	0.26	0.35	0.33	**0.34**	0.61	0.44	0.61
F8	0.30	**0.16**	0.23	0.30	**0.11**	0.31		0.26	**0.12**	0.21	0.46	0.48	0.36	0.31	0.34	0.70	**0.41**	0.54	0.46
Fp1	0.18	0.26	0.21	**0.11**	0.21	**0.13**	0.33		**0.15**	**0.13**	0.49	0.54	0.31	0.38	0.35	0.66	0.65	0.52	0.59
Fp2	0.28	0.19	0.22	0.21	**0.11**	0.32	**0.13**	**0.15**		**0.13**	0.48	0.49	0.38	0.36	0.37	0.73	0.63	0.60	0.63
Fz	**0.18**	**0.16**	**0.13**	**0.11**	**0.11**	0.91	0.63	**0.74**	**0.55**		0.55	0.67	0.29	0.24	0.24	2.34	2.53	1.21	1.19
O1	0.19	0.20	0.22	0.47	0.47	0.73	0.80	0.75	0.77	0.34		**0.12**	**0.11**	0.13	**0.12**	0.86	1.00	**0.33**	0.56
O2	0.26	0.22	0.25	0.47	0.44	0.75	0.78	0.74	0.70	0.36	**0.10**		0.14	**0.11**	**0.13**	0.76	0.70	0.33	**0.21**
P3	**0.11**	0.16	**0.13**	0.29	0.33	0.58	0.75	0.68	0.78	0.24	**0.23**	0.40		0.12	**0.10**	**1.79**	1.43	**1.41**	1.34
P4	0.16	**0.11**	**0.13**	0.38	0.25	0.79	0.62	0.69	0.74	0.24	0.27	**0.57**	0.12		**0.10**	1.34	**1.79**	1.17	**2.00**
Pz	**0.28**	**0.21**	**0.11**	0.41	0.36	0.81	0.85	0.82	0.92	0.26	**1.02**	**2.11**	**0.16**	**0.16**		1.53	2.00	2.63	3.14
T3	**0.18**	0.32	0.34	**0.23**	0.45	**0.15**	0.50	0.27	0.42	0.34	0.27	0.31	**0.24**	0.36	0.37		0.39	**0.15**	0.32
T4	0.31	**0.18**	0.30	0.43	**0.23**	0.50	**0.17**	0.44	0.29	0.31	0.32	0.28	0.33	**0.25**	0.34	0.36		0.30	**0.15**
T5	**0.20**	0.32	0.34	0.44	0.58	0.52	0.65	0.59	0.70	0.44	**0.12**	0.19	**0.14**	0.32	0.31	**0.27**	0.59		0.30
T6	0.34	**0.19**	0.33	0.57	0.46	0.76	0.60	0.65	0.64	0.43	0.22	**0.13**	0.27	**0.14**	0.30	0.53	**0.25**	0.26	

Keeping in mind that these upper bound values have a minimal value of $\alpha = 0.10$ although the actual FDR can be as low as 0.00, we consider any $\widehat{FDR}$ between 0.10 and 0.20 to be acceptable. This limit, together with the other rejection criteria used at the single-trial level (statistical outliers, threshold on the SD) and at the average level (threshold on the SD, minimum number of unrejected propagations), provides a sufficiently conservative rejection mechanism. Using this criterion, most adjacent electrodes (bold underlined values in Table 2) seem associated with true relationships (i.e., not fortuitous associations produced by false

detections), although there are some notable exceptions. Most non-adjacent electrodes in Table 2 have an average $\widetilde{FDR}$ higher than 0.2 and are probably not reliably estimated because of high probability of FP; exceptions are highlighted in grey in the table.

As for $\overline{\Delta_t^*}$ and $sd(\Delta_t^*)$, the average and the standard deviation of $\widetilde{FDR}$ ($\overline{\widetilde{FDR}}$ and $sd(\widetilde{FDR})$ respectively) are strongly correlated. For this reason, SDs are not reported but can be estimated using the equation $sd\left(\widetilde{FDR}\right) = 0.715\overline{\widetilde{FDR}} - 0.106$. The regression line approximates these data with $R^2 = 0.91$, a very good approximation as can be appreciated in Figure 6.

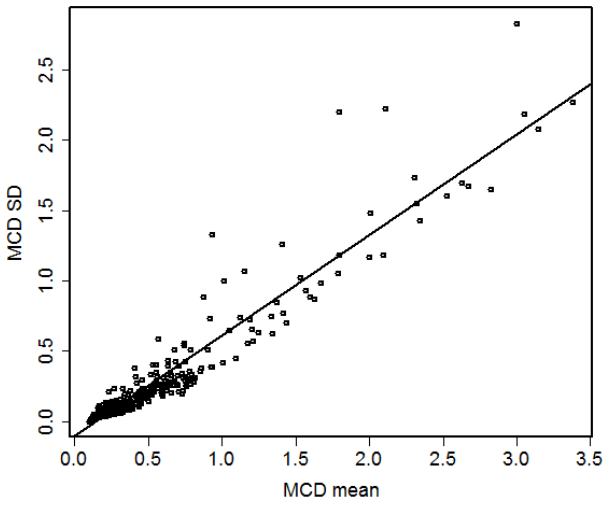

Figure 6. Linear relationship between the average and standard deviation of $\widetilde{FDR}$, computed across the 32 recording nights. The solid line shows the regression $sd\left(\widetilde{FDR}\right) = 0.715 * \overline{\widetilde{FDR}} - 0.106$.

4.5. Topographic distribution of propagation delays

Figure7 shows a map of the propagation delays computed between all adjacent electrodes averaged over the 32 recording nights. Arrowheads indicate propagation direction whereas arrow color varies with propagation delay.

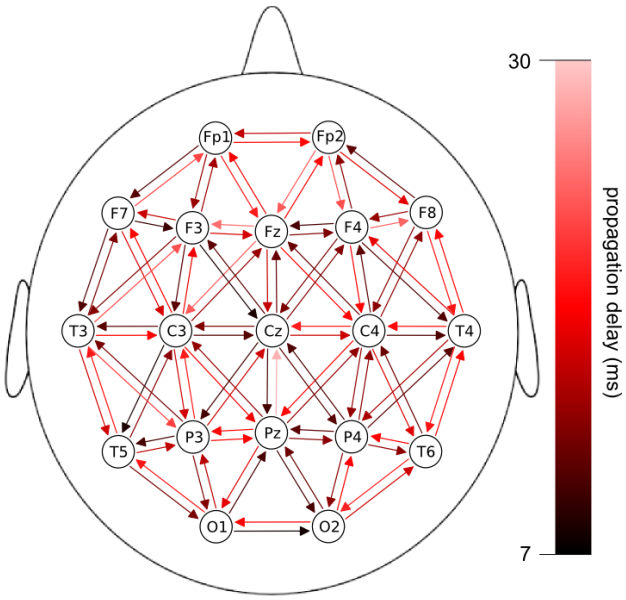

Figure 7. Average propagation delays between adjacent electrodes for 32 recording nights.

As indicated by different-colored arrow pairs, propagation delays are very asymmetric for propagation delays of opposing direction between many channels. For example, pair Cz-Pz delays are minimal (~7 ms) for spindles in the antero-posterior direction but maximal (~30 ms) for spindles propagating in the opposite direction. These asymmetries seem to be quite reliable from subject to subject as can be seen in Figure 8 which displays the same propagation map, but for four typical subjects. Between-subject correlations (Spearman) for the delays reported on these maps were computed for every pair of subjects and are reported in Table 3. These correlations are generally very high (minimum: 0.00; maximum: 0.85; median: 0.64; mean: 0.59; standard deviation: 0.17).

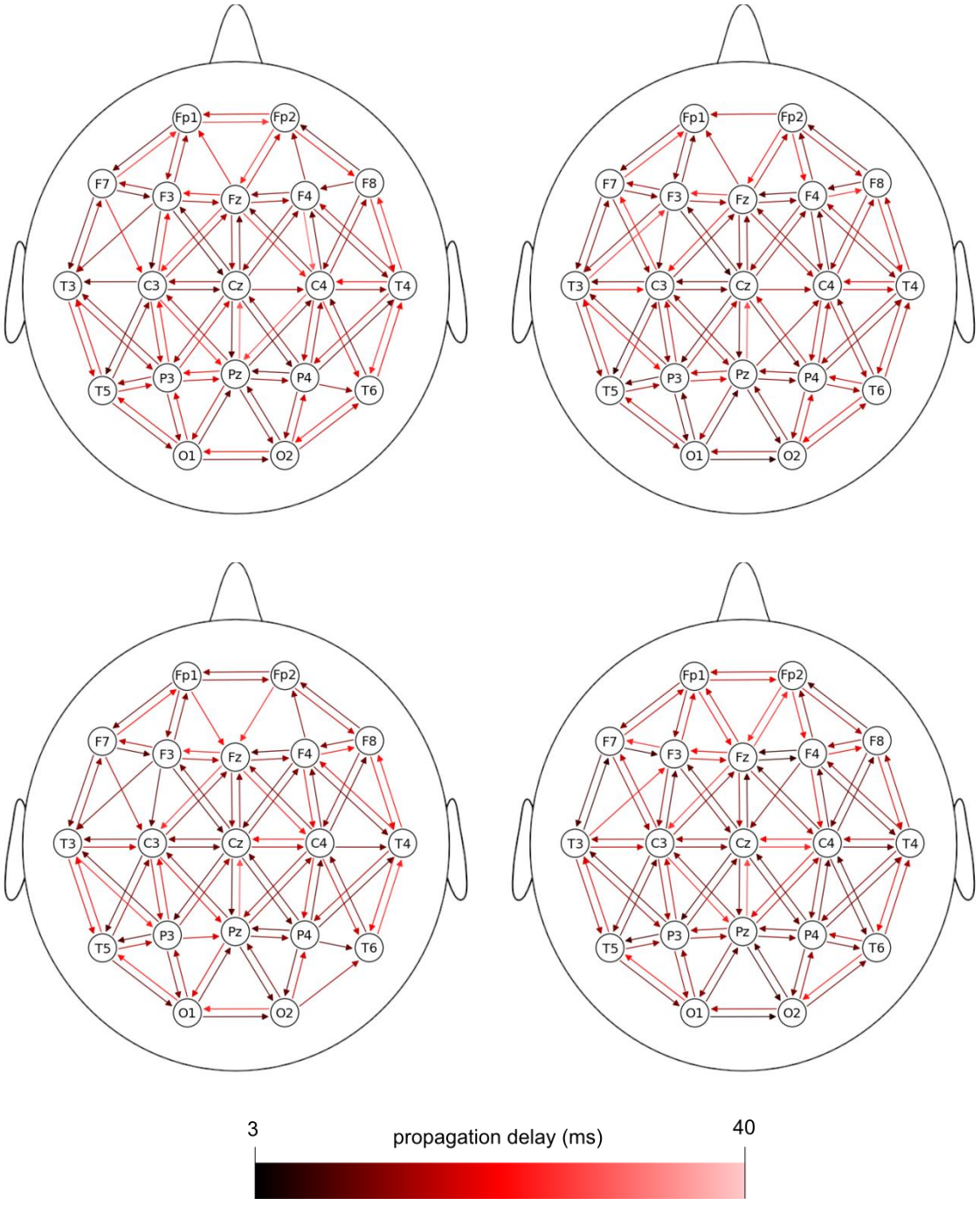

Figure 8. Average propagation delays between adjacent electrodes for four typical subjects. Some arrows are missing because the associated $\overline{\Delta_t^*}$ were not reliable according to the rejection criteria discussed in section 3.

Table 3. Between-subject correlations (Spearman) of propagation delays (between adjacent electrodes only). Correlations for every pair of subjects, numbered from 1 to 17 are reported. The mean correlation for each subject is reported in the last row.

	1	2	3	4	5	6	7	8	9	10	11	12	13	14	15	16	17
1		0.25	0.28	0.37	0.45	0.43	0.33	0.15	0.46	0.12	0.32	0.00	0.30	0.25	0.10	0.26	0.32
2	0.25		0.55	0.56	0.47	0.32	0.72	0.68	0.66	0.59	0.67	0.60	0.63	0.69	0.73	0.51	0.57
3	0.28	0.55		0.71	0.62	0.51	0.77	0.65	0.74	0.52	0.77	0.70	0.71	0.70	0.73	0.73	0.71
4	0.37	0.56	0.71		0.53	0.49	0.67	0.57	0.75	0.61	0.59	0.64	0.69	0.70	0.73	0.62	0.71
5	0.45	0.47	0.62	0.53		0.60	0.55	0.44	0.58	0.54	0.42	0.44	0.57	0.58	0.46	0.62	0.48
6	0.43	0.32	0.51	0.49	0.60		0.38	0.35	0.51	0.42	0.36	0.34	0.47	0.39	0.34	0.50	0.36
7	0.33	0.72	0.77	0.67	0.55	0.38		0.75	0.85	0.65	0.78	0.69	0.75	0.81	0.77	0.68	0.72
8	0.15	0.68	0.65	0.57	0.44	0.35	0.75		0.74	0.63	0.74	0.69	0.73	0.81	0.76	0.73	0.63
9	0.46	0.66	0.74	0.75	0.58	0.51	0.85	0.74		0.70	0.71	0.64	0.80	0.83	0.77	0.71	0.72
10	0.12	0.59	0.52	0.61	0.54	0.42	0.65	0.63	0.70		0.56	0.67	0.70	0.70	0.62	0.67	0.53
11	0.32	0.67	0.77	0.59	0.42	0.36	0.78	0.74	0.71	0.56		0.63	0.65	0.80	0.74	0.73	0.53
12	0.00	0.60	0.70	0.64	0.44	0.34	0.69	0.69	0.64	0.67	0.63		0.73	0.74	0.69	0.66	0.64
13	0.30	0.63	0.71	0.69	0.57	0.47	0.75	0.73	0.80	0.70	0.65	0.73		0.75	0.65	0.76	0.64
14	0.25	0.69	0.70	0.70	0.58	0.39	0.81	0.81	0.83	0.70	0.80	0.74	0.75		0.79	0.78	0.67
15	0.10	0.73	0.73	0.73	0.46	0.34	0.77	0.76	0.77	0.62	0.74	0.69	0.65	0.79		0.67	0.78
16	0.26	0.51	0.73	0.62	0.62	0.50	0.68	0.73	0.71	0.67	0.73	0.66	0.76	0.78	0.67		0.66
17	0.32	0.57	0.71	0.71	0.48	0.36	0.72	0.63	0.72	0.53	0.53	0.64	0.64	0.67	0.78	0.66	
M	*0.27*	*0.58*	*0.65*	*0.62*	*0.52*	*0.42*	*0.68*	*0.63*	*0.70*	*0.58*	*0.63*	*0.59*	*0.66*	*0.69*	*0.65*	*0.64*	*0.60*

5. Conclusion and future directions

In this first paper of a two-part series, we present a new method for tracking and describing the propagation of EEG sleep spindles based on the S-transform and temporal cross-correlation of time-frequency representations. Although the manipulations this procedure requires may seem complex, once the algorithm is implemented it is straightforward to use and well-suited for any standard polysomnographic recordings that use a sufficiently dense array of electrodes (e.g., our 19-electrode 10-20 grid). To facilitate the adoption of this methodology by interested

investigators, its software implementation is available as an open source Python package known as Spyndle.

A short illustration of our method's application was provided and demonstrates that the technique produces reliable results as indicated by the clear inter-subject repeatability of propagation patterns computed across the limited number of subjects and night recordings available. A more comprehensive experimental evaluation has also been performed and is reported in the second part of this series (O'Reilly and Nielsen, 2013a).

Currently, the hypothesis supporting use of a non-null Δ_{sp} padding has not been completely validated. Since this padding adds to the computational load, it might be interesting to cancel out the value of Δ_{sp} if it does not have a significant impact on propagation assessment. Future work will need to address the usefulness of a non-null Δ_{sp} padding to decide this issue. Another topic needing further study is the impact of the p-norm used in $L_p(x, y)$. Most importantly, comparison of spindle propagations computed under the infinity (5) and Euclidean (6) norms might be enlightening on the nature of EEG spindle propagation.

Choice of the best EEG electrode referencing scheme for quantifying time delays with this technique is also a topic requiring more consideration. Some have argued that a surface Laplacian montage provides better accuracy than the common reference montage used in our investigation (Bortel and Sovka, 2013). The Laplacian montage is noted for removing volume conduction effects (Bortel and Sovka, 2013) and muscular artifacts (Fitzgibbon et al., 2013) but also scrambles phase differences (Thatcher, 2012). Although optimal results could be obtained using a high-density electrode montage and anatomical information gathered from magnetic resonance, these methods are not typically used in polysomnographic recordings. To what extend a smaller montage such as the 19-electrode montage used here complemented with

standard head measurements could benefit from a Laplacian montage in the context of the proposed propagation detection methodology requires further investigation.

As a new approach, further validational study is needed. This includes assessment of the functional relevance of the propagation pattern in various clinical disorders, as a function of developmental milestones, in response to novel learning and memory challenges, and with variations in subject traits and demographics. A first step in this direction is taken in (O'Reilly and Nielsen, 2013a).

The proposed methodology was developed specifically for sleep spindle propagation, but it could as easily be applied to any transient EEG phenomenon (O'Reilly and Nielsen, 2013c). It constitutes a new tool for non-invasively tracking discrete EEG events and may help in enhancing our understanding of relationships between EEG signals and brain neurophysiology, especially, spindle-related processes of learning and memory consolidation.

Acknowledgements

The authors thank Tyna Paquette for technical assistance. The research was supported by grants from the Natural Sciences and Engineering Research Council of Canada and the Canadian Institutes of Health Research.

Appendix – Proof that equation (3) is normalized to the unit range using the L_2 norm

Considering $x(t)$ and $y(t)$ as being two positive real valued functions, the Cauchy–Schwarz inequality tells us that

$$\left(\int x(t)y(t)dt\right)^2 \leq \int x^2(t)dt \int y^2(t)dt \tag{13}$$

We can further show that

$$\int x^2(t)dt \int y^2(t)dt \leq \left(\int x^2(t)dt\right)^2 + \left(\int y^2(t)dt\right)^2 \tag{14}$$

by showing that the converse inequality is impossible. To simplify the notation, we define $X \equiv \int x^2(t)dt$ and $Y \equiv \int y^2(t)dt$. Thus, the converse inequality is $XY > X^2 + Y^2$ which implies that $0 > X^2 + Y^2 - XY \geq X^2 + Y^2 - 2XY = (X - Y)^2$, which is impossible since $(X - Y)^2 \geq 0$, X and Y being two real positive variables. Thus, by *reductio ad absurdum*, (14) is necessarily true, and thus $(\int x(t)y(t)dt)^2 \leq (\int x^2(t)dt)^2 + (\int y^2(t)dt)^2$ is also true. This reasoning can be applied with integration in N dimensions, as the Cauchy–Schwarz inequality can be formulated in N dimensions and the rest of the demonstration does not depend on the fact that X or Y values are obtained through integration. Thus, replacing $x(t)$ and $y(t)$ by $|S_R(t,f)|$ and $|S_T(t+\Delta_t,f)|$, integrating along both temporal and frequency axes, and applying some basic algebra, we obtain

$$\frac{\left|\widetilde{S_R}(0)\right| \star \left|\widetilde{S_T}(\Delta_t)\right|}{L_p(\left|\widetilde{S_R}(0)\right|,\ \left|\widetilde{S_T}(\Delta_t)\right|)} \leq 1$$

The fact that $\frac{|\widetilde{S_R}(0)|\star|\widetilde{S_T}(\Delta_t)|}{L_p(|\widetilde{S_R}(0)|,|\widetilde{S_T}(\Delta_t)|)} \geq 0$ is trivial by the fact that $|S_R(t,f)|$ and $|S_T(t+\Delta_t,f)|$ are positive real valued functions. ■

References

Allena M, Campus C, Morrone E, De Carli F, Garbarino S, Manfredi C, Sebastiano DR, Ferrillo F. Periodic limb movements both in non-REM and REM sleep: relationships between cerebral and autonomic activities. Clin Neurophysiol, 2009; 120: 1282-90.

Anderer P, Klosch G, Gruber G, Trenker E, Pascual-Marqui RD, Zeitlhofer J, Barbanoj MJ, Rappelsberger P, Saletu B. Low-resolution brain electromagnetic tomography revealed simultaneously active frontal and parietal sleep spindle sources in the human cortex. Neuroscience, 2001; 103: 581-92.

Andrillon T, Nir Y, Staba RJ, Ferrarelli F, Cirelli C, Tononi G, Fried I. Sleep spindles in humans: insights from intracranial EEG and unit recordings. J Neurosci, 2011; 31: 17821-34.

Assous S, Boashash B. Evaluation of the modified S-transform for time-frequency synchrony analysis and source localisation. EURASIP J Adv Signal Process, 2012; 2012: 49.

Baillet S, Mosher JC, Leahy RM. Electromagnetic brain mapping. IEEE Signal Process Mag, 2001; 18: 14-30.

Bortel R, Sovka P. Potential approximation in realistic Laplacian computation. Clin Neurophysiol, 2013; 124: 462-73.

Brown RA, Lauzon ML, Frayne R. A General Description of Linear Time-Frequency Transforms and Formulation of a Fast, Invertible Transform That Samples the Continuous S-Transform Spectrum Nonredundantly. IEEE Trans Signal Process, 2010; 58: 281-90.

Campbell K, Kumar A, Hofman W. Human and automatic validation of a phase-locked loop spindle detection system. Electroencephalogr Clin Neurophysiol, 1980; 48: 602-5.

Caporro M, Haneef Z, Yeh HJ, Lenartowicz A, Buttinelli C, Parvizi J, Stern JM. Functional MRI of sleep spindles and K-complexes. Clin Neurophysiol, 2012; 123: 303-9.

Crowley K, Trinder J, Kim Y, Carrington M, Colrain IM. The effects of normal aging on sleep spindle and K-complex production. Clin Neurophysiol, 2002; 113: 1615-22.

Dang-Vu TT, McKinney SM, Buxton OM, Solet JM, Ellenbogen JM. Spontaneous brain rhythms predict sleep stability in the face of noise. Curr Biol, 2010; 20: R626-7.

De Gennaro L, Ferrara M. Sleep spindles: an overview. Sleep Med Rev, 2003; 7: 423-40.

Dehghani N, Cash SS, Halgren E. Emergence of synchronous EEG spindles from asynchronous MEG spindles. Hum Brain Mapp, 2011a; 32: 2217-27.

Dehghani N, Cash SS, Halgren E. Topographical frequency dynamics within EEG and MEG sleep spindles. Clin Neurophysiol, 2011b; 122: 229-35.

Doran SM. The Dynamic Topography of Individual Sleep Spindles. Sleep Res Online, 2003; 5: 133-9.

Ferrarelli F, Peterson MJ, Sarasso S, Riedner BA, Murphy MJ, Benca RM, Bria P, Kalin NH, Tononi G. Thalamic dysfunction in schizophrenia suggested by whole-night deficits in slow and fast spindles. Am J Psychiatry, 2010; 167: 1339-48.

Fitzgibbon SP, Lewis TW, Powers DM, Whitham EW, Willoughby JO, Pope KJ. Surface laplacian of central scalp electrical signals is insensitive to muscle contamination. IEEE Trans Biomed Eng, 2013; 60: 4-9.

Flandrin P. A time-frequency formulation of optimum detection. IEEE Trans Acoust, 1988; 36: 1377-84.

Fogel SM, Smith CT. The function of the sleep spindle: a physiological index of intelligence and a mechanism for sleep-dependent memory consolidation. Neurosci Biobehav Rev, 2011; 35: 1154-65.

Fraiwan L, Lweesy K, Khasawneh N, Wenz H, Dickhaus H. Automated sleep stage identification system based on time-frequency analysis of a single EEG channel and random forest classifier. Comput Methods Programs Biomed, 2011.

Granger CWJ. Investigating Causal Relations by Econometric Models and Cross-spectral Methods. Econometrica, 1969; 37: 424-38.

Grave de Peralta Menendez R, Gonzalez Andino SL, Morand S, Michel CM, Landis T. Imaging the electrical activity of the brain: ELECTRA. Hum Brain Mapp, 2000; 9: 1-12.

Iber C, Ancoli-Israel S, Chesson a, Quan SF. The AASM Manual for the Scoring of Sleep and Associated Events: Rules, Terminology and Technical Specifications. American Academy of Sleep Medicine: Westchester, IL, 2007.

Jones KA, Porjesz B, Chorlian D, Rangaswamy M, Kamarajan C, Padmanabhapillai A, Stimus A, Begleiter H. S-transform time-frequency analysis of P300 reveals deficits in individuals diagnosed with alcoholism. Clin Neurophysiol, 2006; 117: 2128-43.

Kaminski MJ, Blinowska KJ. A new method of the description of the information flow in the brain structures. Biol Cybern, 1991; 65: 203-10.

Knoblauch V, Martens WL, Wirz-Justice A, Cajochen C. Human sleep spindle characteristics after sleep deprivation. Clin Neurophysiol, 2003; 114: 2258-67.

Kokkinos V, Koupparis A, Stavrinou ML, Kostopoulos GK. The hypnospectrogram: an EEG power spectrum based means to concurrently overview the macroscopic and microscopic architecture of human sleep. J Neurosci Methods, 2009; 185: 29-38.

Ktonas PY, Golemati S, Xanthopoulos P, Sakkalis V, Ortigueira MD, Tsekou H, Zervakis M, Paparrigopoulos T, Bonakis A, Economou NT, Theodoropoulos P, Papageorgiou SG, Vassilopoulos D, Soldatos CR. Time-frequency analysis methods to quantify the time-varying microstructure of sleep EEG spindles: possibility for dementia biomarkers? J. Neurosci Methods, 2009; 185: 133-42.

Massimini M, Huber R, Ferrarelli F, Hill S, Tononi G. The sleep slow oscillation as a traveling wave. J Neurosci, 2004; 24: 6862-70.

Michel CM, Murray MM, Lantz G, Gonzalez S, Spinelli L, Grave de Peralta R. EEG source imaging. Clin Neurophysiol, 2004; 115: 2195-222.

Molle M, Bergmann TO, Marshall L, Born J. Fast and slow spindles during the sleep slow oscillation: disparate coalescence and engagement in memory processing. Sleep, 2011; 34: 1411-21.

Morrow TJ, Casey KL. A microprocessor device for the real-time detection of synchronized alpha and spindle activity in the EEG. Brain Res Bull, 1986; 16: 439-42.

Murakami S, Okada Y. Contributions of principal neocortical neurons to magnetoencephalography and electroencephalography signals. J Physiol, 2006; 575: 925-36.

Nolte G, Bai O, Wheaton L, Mari Z, Vorbach S, Hallett M. Identifying true brain interaction from EEG data using the imaginary part of coherency. Clin Neurophysiol, 2004; 115: 2292-307.

Nunez PL, Srinivasan R. Electric fields of the brain the neurophysics of EEG, 2nd ed. Oxford University Press: Oxford, 2006.

O'Reilly C, Nielsen T. Assessing EEG sleep spindle propagation. Part 2 : Experimental characterization. Submitted to J Neurosci Methods, 2013a.

O'Reilly C, Nielsen T. Revisiting the ROC curve for diagnostic applications with an unbalanced class distribution. The 9th international Workshop on Systems, Signal Processing and their Applications: Special Sessions: Mazafran, Algeria, 2013b: 363-70.

O'Reilly C, Nielsen T. Sleep spindle detection: Automatic detection and evaluation of performance with a fine temporal resolution. Submitted to IEEE Trans Biomed Eng, 2013c.

O'Toole J, Mesbah M, Boashash B. Neonatal eeg seizure detection using a time-frequency matched filter with a reduced template set. Proceedings of the Eighth International Symposium on Signal Processing and Its Applications, 2005: 215-8.

Pinnegar CR, Khosravani H, Federico P. Time-frequency phase analysis of ictal EEG recordings with the S-transform. IEEE Trans Biomed Eng, 2009; 56: 2583-93.

Plonsey R. The nature of sources of bioelectric and biomagnetic fields. Biophys J, 1982; 39: 309-12.

Ray LB, Fogel SM, Smith CT, Peters KR. Validating an automated sleep spindle detection algorithm using an individualized approach. Journal of sleep research, 2010; 19: 374-8.

Rousseeuw P, Van Driessen K. A fast algorithm for the minimum covariance determinant estimator. Technometrics, 1999; 41: 212-23.

Salmelin R, Baillet S. Electromagnetic brain imaging. Hum. Brain Mapp., 2009; 30: 1753-7.

Sameshima K, Baccala LA. Using partial directed coherence to describe neuronal ensemble interactions. J Neurosci Methods, 1999; 94: 93-103.

Schabus M, Dang-Vu TT, Albouy G, Balteau E, Boly M, Carrier J, Darsaud A, Degueldre C, Desseilles M, Gais S, Phillips C, Rauchs G, Schnakers C, Sterpenich V, Vandewalle G, Luxen A, Maquet P. Hemodynamic cerebral correlates of sleep spindles during human non-rapid eye movement sleep. Proc Natl Acad Sci U. S. A., 2007; 104: 13164-9.

Schabus M, Dang-Vu TT, Heib DP, Boly M, Desseilles M, Vandewalle G, Schmidt C, Albouy G, Darsaud A, Gais S, Degueldre C, Balteau E, Phillips C, Luxen A, Maquet P. The Fate of Incoming Stimuli during NREM Sleep is Determined by Spindles and the Phase of the Slow Oscillation. Front Neurol, 2012; 3: 40.

Schabus M, Gruber G, Parapatics S, Sauter C, Klosch G, Anderer P, Klimesch W, Saletu B, Zeitlhofer J. Sleep spindles and their significance for declarative memory consolidation. Sleep, 2004; 27: 1479-85.

Schabus M, Hodlmoser K, Gruber G, Sauter C, Anderer P, Klosch G, Parapatics S, Saletu B, Klimesch W, Zeitlhofer J. Sleep spindle-related activity in the human EEG and its relation to general cognitive and learning abilities. Eur J Neurosci, 2006; 23: 1738-46.

Schimicek P, Zeitlhofer J, Anderer P, Saletu B. Automatic sleep-spindle detection procedure: aspects of reliability and validity. Clinical EEG, 1994; 25: 26-9.

Senapati K, Routray A. Comparison of ICA and WT with S-transform based method for removal of ocular artifact from EEG signals. J Biomed Sci Eng, 2011; 4: 341-51.

Stam CJ, Nolte G, Daffertshofer A. Phase lag index: assessment of functional connectivity from multi channel EEG and MEG with diminished bias from common sources. Hum Brain Mapp, 2007; 28: 1178-93.

Stam CJ, van Dijk BW. Synchronization likelihood: an unbiased measure of generalized synchronization in multivariate data sets. Phys Nonlinear Phenom, 2002; 163: 236-51.

Steriade M. Corticothalamic resonance, states of vigilance and mentation. Neuroscience, 2000; 101: 243-76.

Stockwell RG, Mansinha L, Lowe RP. Localization of the complex spectrum: the S transform. IEEE Trans Signal Process, 1996; 44: 998-1001.

Tamaki M, Matsuoka T, Nittono H, Hori T. Fast sleep spindle (13-15 hz) activity correlates with sleep-dependent improvement in visuomotor performance. Sleep, 2008; 31: 204-11.

Tarokh L, Carskadon MA. Developmental changes in the human sleep EEG during early adolescence. Sleep, 2010; 33: 801-9.

Thatcher RW. Coherence, phase differences, phase shift, and phase lock in EEG/ERP analyses. Dev Neuropsychol, 2012; 37: 476-96.

Tukey JW. Exploratory data analysis. Addison-Wesley Pub. Co.: Reading, Mass. ; Don Mills, Ont., 1977.

Tyvaert L, Levan P, Grova C, Dubeau F, Gotman J. Effects of fluctuating physiological rhythms during prolonged EEG-fMRI studies. Clin Neurophysiol, 2008; 119: 2762-74.

van der Helm E, Gujar N, Nishida M, Walker MP. Sleep-dependent facilitation of episodic memory details. PloS one, 2011; 6: e27421.

Ventouras EM, Ktonas PY, Tsekou H, Paparrigopoulos T, Kalatzis I, Soldatos CR. Independent Component Analysis for Source Localization of EEG Sleep Spindle Components. Comput Intell Neurosci, 2010; doi: 10.1155/2010/329436.

Wamsley EJ, Tucker MA, Shinn AK, Ono KE, McKinley SK, Ely AV, Goff DC, Stickgold R, Manoach DS. Reduced sleep spindles and spindle coherence in schizophrenia: mechanisms of impaired memory consolidation? Biol Psychiatry, 2012; 71: 154-61.